

Article

Sensorless PMSM Drive Implementation by Introduction of Maximum Efficiency Characteristics in Reference Current Generation

Željko Plantić¹, Tine Marčič², Miloš Beković³ and Gorazd Štumberger^{3,*} ¹ Energy Institute Hrvoje Požar, 10001 Zagreb, Croatia; zplantic@eihp.hr² Energy Agency of the Republic of Slovenia, 2000 Maribor, Slovenia; tine.marcic@agen-rs.si³ Power engineering institute, Faculty of Electrical Engineering and Computer Science; University of Maribor, 2000 Maribor, Slovenia; milos.bekovic@um.si

* Correspondence: gorazd.stumberger@um.si; Tel.: +386-2220-7075

Received: 31 July 2019; Accepted: 5 September 2019; Published: 11 September 2019



Abstract: This paper presents the efficiency improvement in a speed closed-loop controlled permanent magnet synchronous machine (PMSM) sensorless drive. The drive efficiency can be improved by minimizing the inverter and the PMSM losses. These can be influenced by proper selection of DC-bus voltage and switching frequency of the inverter. The direct (d-) and quadrature (q-) axis current references generation methods, discussed in this paper, further improve the efficiency of the drive. Besides zero d-axis current reference control, the maximum torque per ampere (MTPA) characteristic is normally applied to generate the d- and q-axis current references in vector controlled PMSM drives. It assures control with maximum torque per unit of current but cannot assure maximum efficiency. In order to improve efficiency of the PMSM drive, this paper proposes the generation of d- and q-axis current references based on maximum efficiency (ME) characteristic. In the case study, the MTPA and ME characteristics are theoretically evaluated and determined experimentally by measurements on discussed PMSM drive. The obtained characteristics are applied for the d- and q-axis current references generation in the speed closed-loop vector controlled PMSM drive. The measured drive efficiency clearly shows that the use of ME characteristic instead of MTPA characteristic or zero d-axis current in the current references generation improves the efficiency of PMSM drive realizations with position sensor and without it—sensorless control.

Keywords: magnetic loss; maximum efficiency (ME) characteristic; maximum torque per ampere (MTPA) characteristic; modeling; permanent magnet synchronous machine (PMSM); sensorless control

1. Introduction

The energy savings during the entire exploitation time of an electric drive can be achieved only through a coordinated efficiency improvement of all components of the drive, including control algorithms. Nowadays, efficiency maximization is a normal design aspect for electric drives. Thus, more and more researchers are occupied with decreasing overall power losses of electric drives and simultaneously saving component and operational costs. In some applications, minimum loss is not only one of the design criteria, but is of paramount importance, e.g., in battery-powered road-vehicles [1,2] or even more importantly in autonomous aircrafts [3]. In such applications, even a small decrease of losses can have a significant impact on overall system performance in terms of ensuring adequate operating range. Due to its high efficiency, high power density and wide operating range of speed, the permanent magnet synchronous machine (PMSM) is used very often. By employment of a speed- or position-sensorless control, a more compact drive with less maintenance [4–6] can be obtained.

Besides designing a new machine, the efficiency of the drive can be improved by minimizing losses of the power inverter by proper selection of the DC-bus voltage and the switching frequency [7–9], and a proper control of the PMSM as well. Sensorless PMSM drive control algorithms vary in complexity and computational performance demanded by different target applications. The main difference between available sensorless control algorithms from the literature is that model-based methods [5,10–13] are more straightforward to implement but are not directly applicable at standstill, and therefore saliency-based methods [14–16] have been developed. Authors combine the aforementioned methods in various approaches [9,17–20], thus ensuring adequate sensorless performance from zero speed up to the field-weakening region.

In the case of vector controlled PMSM, a proper selection of the direct (d-) and quadrature (q-) axis current references can further improve drive efficiency. The simplest zero d-axis current reference control ($i_{dr} = 0$) is still employed in applications with surface mounted PMSMs [21], which exhibit similar values of d- and q-axis inductances. Although it is generally applicable, the maximum torque per ampere (MTPA) characteristic [10,15,19–27], which considers PMSM copper losses, is usually used for generation of current references in drives with interior PMSM, which exhibit different values of d- and q-axis inductances and thus produce a significant reluctance torque component in addition to the permanent magnet torque component. When MTPA is applied, the PMSM drive produces maximum torque per unit of stator current but cannot reach the maximum efficiency due to the neglected iron core losses. The maximum efficiency (ME) characteristic [21,23–28] considers copper losses as well as iron core losses of PMSM. When it is applied for generation of current references, the maximum efficiency of a PMSM drive can be achieved. The concept was first evaluated by Colby et al. [29] for a surface mounted PMSM. Later it was applied by Morimoto et al. [30] in control of an interior PMSM drive as well. More recently, Pohlenz et al. [23] and Cavallaro et al. [28] reported improved efficiencies by implementing ME in the control software. While applying ME, Hassan et al. [24] analyzed PMSM and inverter losses due to changed harmonic content. Ni et al. [21] developed an iron loss formula by introducing new coefficients. However, the needed detailed PMSM data might not always be available, as discussed later.

General forms of the MTPA characteristic and the ME characteristic are shown in Figure 1a, from where it is evident that ME characteristics require higher values of the negative d-axis current in comparison to the MTPA characteristics, and MTPA characteristics in turn require higher values of the negative d-axis current than the $i_{dr} = 0$ control. Figure 1b shows the stator current vector \mathbf{I}_s and its components I_d and I_q , where $|\mathbf{I}_s|$ denotes the length of \mathbf{I}_s .

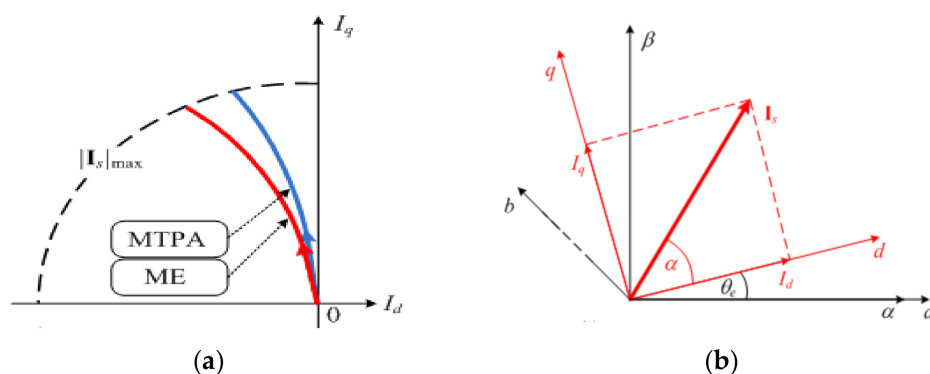


Figure 1. Maximum torque per ampere (MTPA) and maximum efficiency (ME) characteristics (a) and stator current vector in α - β and d-q reference frame (b).

In this paper, the origins of losses in a PMSM drive are introduced and evaluated in Section 2. The PMSM model is used to explain the differences between the MTPA and ME characteristics, and to obtain the equations which relate the ME characteristics to the stator currents I_d and I_q in Section 3. Although the ME characteristics are usually derived in relation to the magnetizing currents I_{md} and I_{mq} ,

the here presented Equation (20) provides the optimal current I_d for a given load torque by considering the ME characteristic—i.e., the copper and the iron losses of the PMSM. Furthermore, this paper focuses on the drive implementation from the control designer's point of view, where detailed information of the PMSM is not available, contrarily to machine designer's point of view, where all details of the PMSM are known [21]. Unfortunately, the aforementioned equations cannot be used directly in the control implementation because the needed iron core resistance parameter value R_c cannot be determined directly or to be modeled in form of a function. Therefore, this paper proposes an alternative, which is suitable for control design and applicable to all types of PMSM. There the ME characteristics are determined experimentally by measurements performed on the tested vector controlled PMSM drive. The existing control algorithm is extended by a current references generator, where the determined ME characteristics are applied to generate the d- and q-axis current references. The speed closed-loop vector control of PMSM, obtained in this way, is used to measure the efficiency of the entire drive. The control is realized with the position sensor and without it—sensorless control.

Moreover, in this work the ME characteristics are implemented in sensorless control for the first time and presented in Section 4. There the rotor speed and position are determined by nonlinear phase-locked loop (PLL) observer [9,31], whose inputs are calculated by the modified active flux method [32–35]. It is shown that the drive efficiency can be improved when ME characteristics are used to generate the d- and q-axis current references, which is true for the sensorless control as well as for the control realization with position sensor. In order to facilitate a direct comparison, the space vector modulation has been utilized without any advanced modulation techniques such as discussed in [36,37]. Section 5 then concludes the paper.

2. PMSM Drive Losses

A PMSM drive normally consists of the PMSM, power inverter, load, and the control system. The load is the element, which dictates the proper selection of the other PMSM drive elements. The energy conversion process inevitably includes losses, mostly in the power inverter and PMSM. These loss components substantially influence the drive efficiency. This paper focuses on the detailed research of PMSM losses, which are minimized in the speed closed-loop controlled PMSM drive by a proper generation of d- and q-axis current references.

The employed PMSM had surface mounted magnets and was rated for 400 V and 1.6 kW at 2250 rpm.

2.1. Power Losses in Power Inverter

The power losses in a power inverter consist of conduction or Ohm's losses and switching losses. In this work they are minimized by proper selection of the DC-bus voltage, where the impact of dead times is minimized [5,8,9] and by proper selection of the switching frequency [7,24,36,37] as well. The proper values were determined experimentally by measurements performed on the tested PMSM drive.

In order to evaluate the impact of switching frequency on drive efficiency, a series of tests was performed, where the PMSM load was varied, while the switching frequency was set to 4, 6, and 9 kHz, respectively. Figure 2 presents the PMSM drive efficiency characteristics in dependence of the current vector length $|i_s|$. Drive efficiencies vary because the inverter losses increase with the increase of switching frequency and simultaneously the PMSM losses decrease with the increase of switching frequency [38], and the drive efficiency represents their product. Figure 2 shows that the highest efficiency of this particular PMSM drive was obtained when the switching frequency of 6 kHz was employed. Thus, the aforementioned switching frequency value was used through all successive tests.

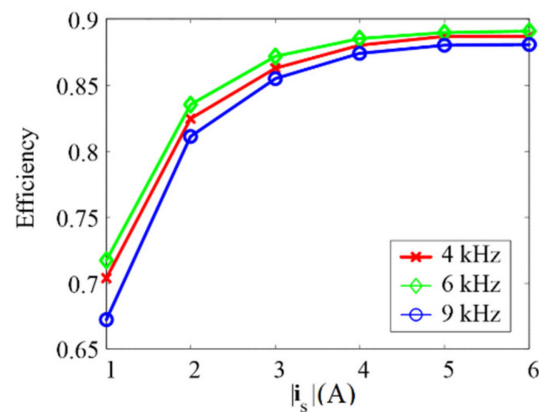


Figure 2. Measured efficiency characteristics of the permanent magnet synchronous machine (PMSM) drive at different switching frequencies.

In addition to the switching frequency, the inverter's DC-bus voltage influences the PMSM drive efficiency as well. When the desired inverter output voltage is much smaller than the DC-bus voltage, then the inverter output voltage pulses are unnecessarily narrow which increases switching losses. However, it is noted that the DC-bus voltage control is not possible if a diode rectifier is employed in the inverter. In order to evaluate the impact of DC-bus voltage on PMSM drive efficiency, a series of tests was performed, where the PMSM load was varied, while the rotor speed and DC-bus voltage were set to different values. The PMSM efficiency was not significantly affected by the change of DC-bus voltage. Thus, the significant variation of PMSM drive efficiency presented in Figure 3 was due to the inverter efficiency variation by the change of DC-bus voltage. The differences in efficiencies at low speeds were more expressed because the PMSM back-emf was smaller at low speeds. The implementation of variable DC-bus voltage could make sense in variable speed drives operating mostly at partial loads and in a broad range of speeds in applications where efficiency is crucial.

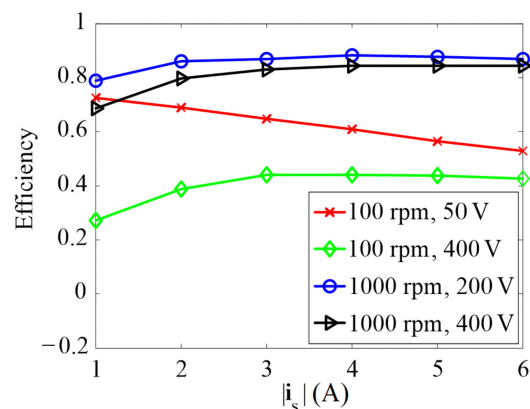


Figure 3. Measured efficiency characteristics of the PMSM drive at different rotor speed and different DC-bus voltage.

2.2. Power Losses in PMSM

The analysis of power losses in the PMSM is based on the two-axis steady-state PMSM model with lumped parameters, written in the d-q reference frame. The d-axis was aligned with the flux linkage vector due to the permanent magnets while the q-axis led for electrical $\pi/2$. The model is schematically shown in Figure 4.

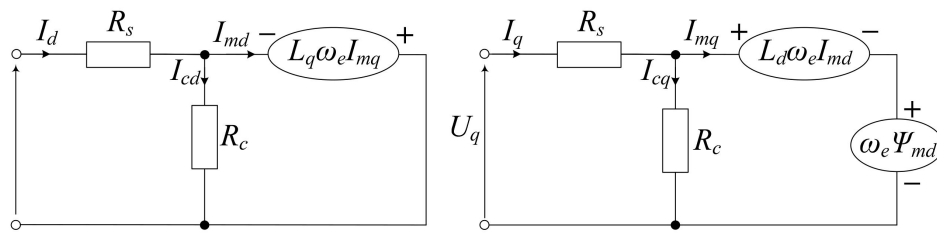


Figure 4. Applied steady-state model of PMSM in d-q reference frame.

The copper losses are considered by the stator resistance R_s while the iron core losses are accounted for by the iron core resistance R_c . In the steady-state model, written in the d-q reference frame, the indices d and q refer to the d- and q-axis, U_d and U_q are the stator voltages, I_d and I_q are stator currents, I_{md} and I_{mq} are the magnetizing currents, I_{cd} and I_{cq} are the iron core currents, L_d and L_q are the stator inductances, Ψ_{md} is the flux linkage due to the permanent magnets, T_e is the electromagnetic torque, ω_e is the electrical rotor speed and p_p is the number of pole pairs. Considering Figure 4, the voltage Equation (1) and the torque Equation (2) can be written:

$$\begin{aligned} U_d &= R_s I_d - \omega_e L_q I_{mq} \\ U_q &= R_s I_q + \omega_e L_d I_{md} + \omega_e \Psi_{md} \end{aligned} \quad (1)$$

$$T_e = p_p I_{mq} (\Psi_{md} + (L_d - L_q) I_{md}) \quad (2)$$

where

$$\begin{aligned} I_d &= I_{md} + I_{cd} = I_{md} - \frac{\omega_e L_q I_{mq}}{R_c} \\ I_q &= I_{mq} + I_{cq} = I_{mq} + \frac{\omega_e}{R_c} (L_d I_{md} + \Psi_{md}) \end{aligned} \quad (3)$$

The power losses in the P_{MMSM} $P_{loss,PMSM}$ can be divided into controllable losses, which are the copper losses $P_{loss,Cu}$ and the iron core losses $P_{loss,Fe}$, and uncontrollable losses, which are the mechanical and additional losses [28]. Neglecting the uncontrollable losses, (4) describes the PMSM losses.

$$P_{loss,PMSM} = P_{loss,Cu} + P_{loss,Fe} \quad (4)$$

Considering Figure 4 and Equations (1) to (4), $P_{loss,Cu}$ and $P_{loss,Fe}$ can be expressed by (5) and (6).

$$P_{loss,Cu} = R_s (I_d^2 + I_q^2) = R_s \left(I_{md} - \frac{\omega_e L_q I_{mq}}{R_c} \right)^2 + R_s \left(I_{mq} + \frac{\omega_e (L_d I_{md} + \Psi_{md})}{R_c} \right)^2 \quad (5)$$

$$P_{loss,Fe} = R_c (I_{cd}^2 + I_{cq}^2) = \frac{\omega_e^2}{R_c} \left[(L_q I_{mq})^2 + (L_d I_{md} + \Psi_{md})^2 \right], \quad (6)$$

3. Improving Efficiency by Reference Current Generation

Assuming a given inverter and a given PMSM, the PMSM drive efficiency can be improved by minimizing inverter losses and PMSM losses. In addition to advanced modulation techniques [36,37], the inverter losses can be mostly influenced by the closed-loop control or a proper choice of DC-bus voltage and by an optimal choice of switching frequency [24]. The PMSM losses can be influenced by the voltage and current total harmonic distortion that depend on the switching frequency [7,24,38], and in the case of vector controlled PMSM by the generation of the d- and q-axis current references. The generation of current references is usually based $i_{dr} = 0$ or on the MTPA characteristic [10,15,19–23], which assures the maximum torque per unit of current but not the maximum efficiency of the entire drive [21,23]. The last can be achieved when the ME characteristic is applied for generation of the d- and q-axis current references.

3.1. Theoretical Background of the MTPA and ME Characteristics

Let us consider all parameters of the PMSM steady-state model, shown in Figure 4 and described by Equations (1) to (6), as constant. The starting point for derivation of the MTPA characteristic is the torque equation (Equation (2)) and the PMSM steady-state model shown in Figure 4, where the iron core resistance is neglected ($R_c \rightarrow \infty$). Consequently, according to Equation (3), I_{cd} and I_{cq} equal zero which leads to $I_d = I_{md}$ and $I_q = I_{mq}$. Considering the angle of the stator current vector α , shown in Figure 1b, the relation between the d- and q-axis currents, that provides the maximum torque per unit of current, can be determined from Equation (2) by Equation (7), which yields Equation (8) [22].

$$\max(T_e) \Rightarrow \frac{dT_e}{d\alpha} = 0 \quad (7)$$

$$I_{d1,2} = \frac{-\Psi_{md}}{2(L_d - L_q)} \pm \sqrt{\frac{\Psi_{md}^2}{4(L_d - L_q)^2} + I_q^2} \quad (8)$$

Similarly, the ME characteristic describes the relation between the d- and q-axis current that provides the minimum of PMSM losses, which leads to the maximum efficiency of the PMSM drive. According to [24,28], the PMSM losses (Equation (4)) can be minimized for each combination of T_e , and ω_e . Considering Equation (2) in Equations (5) and (6), Equation (4) can be expressed as a function of I_{md} , T_e , and ω_e . In the case of steady-state operation, T_e , and ω_e are constants, which means that the PMSM power losses $P_{loss,PMSM}$ (Equation (4)) can be described as a function of I_{md} . However, because T_e (Equation (2)) depends on I_{md} and I_{mq} , the PMSM power losses can be minimized by Equation (9), which yields Equation (10) [24] describing the ME characteristic.

$$\min(P_{loss,PMSM}) \Rightarrow \left. \frac{dP_{loss,PMSM}(I_{md}, I_{mq}, \omega_e)}{dI_{md}} \right|_{T_e, \omega_e} = 0 \quad (9)$$

$$I_{md} = -\frac{\omega_e^2 L_d \Psi_{md} (R_s + R_c) + R_s R_c \omega_e (L_d - L_q) I_{mq}}{\omega_e^2 L_d^2 (R_s + R_c) + R_s R_c^2} \quad (10)$$

3.2. Evaluation of the Impact of R_c on the ME Characteristic

A sensitivity analysis was performed in order to evaluate the impact of the iron core resistance R_c on the ME characteristic. The parameter R_c was varied while the other PMSM parameters presented in Table 1 remained constant. The theoretical derivation of obtaining the necessary measurable current I_d for every corresponding combination of I_q and ω_e is presented hereinafter with the assumption of constant PMSM model parameters in the given operating points.

Table 1. Permanent magnet synchronous machine PMSM parameters.

Parameter	Value
p_p	5
R_s (Ω)	1.15
Ψ_{md} (Vs)	0.2415
L_d (H)	0.02654
L_q (H)	0.02865

The voltage equations derived from Figure 4 can be rewritten also in the form of Equation (11).

$$\begin{aligned} U_d &= R_s I_{md} - \frac{R_s + R_c}{R_c} \omega_e L_q I_{mq} \\ U_q &= R_s I_{mq} + \frac{R_s + R_c}{R_c} (\omega_e L_d I_{md} + \omega_e \Psi_{md}) \end{aligned} \quad (11)$$

Considering Equation (3), the currents I_{md} and I_{mq} can be expressed in terms of the measurable stator currents I_d and I_q (Equation (12)). Note that it is essential for control implementation that measurable quantities (such as I_d and I_q instead of I_{md} and I_{mq}) are included in the algorithm.

$$\begin{aligned} I_{md}(I_d, I_q) &= \frac{R_c^2 I_d + R_c L_q \omega_e I_q - L_q \Psi_{md} \omega_e^2}{R_c^2 + L_d L_q \omega_e^2} \\ I_{mq}(I_d, I_q) &= \frac{R_c^2 I_q - R_c L_d \omega_e I_d - R_c \Psi_{md} \omega_e}{R_c^2 + L_d L_q \omega_e^2} \end{aligned} \quad (12)$$

Similarly, the currents I_{cd} and I_{cq} can be expressed in terms of I_d and I_q (13).

$$\begin{aligned} I_{cd}(I_d, I_q) &= \frac{L_d L_q \omega_e^2 I_d - R_c L_q \omega_e I_q + L_q \Psi_{md} \omega_e^2}{R_c^2 + L_d L_q \omega_e^2} \\ I_{cq}(I_d, I_q) &= \frac{R_c L_d \omega_e I_d + L_d L_q \omega_e^2 I_q + R_c \Psi_{md} \omega_e}{R_c^2 + L_d L_q \omega_e^2} \end{aligned} \quad (13)$$

Then the PMSM losses can be expressed in terms of I_d and I_q as well (14).

$$\begin{aligned} P_{loss, PMSM} &= AI_d^2 + BI_q^2 + CI_d + DI_q + EI_d I_q + F \\ A &= \frac{L_d^2 L_q^2 \omega_e^4 (R_s + R_c) + R_c^2 (R_s R_c^2 + 2R_s L_d L_q \omega_e^2 + R_c L_d^2 \omega_e^2)}{(R_c^2 + L_d L_q \omega_e^2)^2} \\ B &= \frac{L_d^2 L_q^2 \omega_e^4 (R_s + R_c) + R_c^2 (R_s R_c^2 + 2R_s L_d L_q \omega_e^2 + R_c L_d^2 \omega_e^2)}{(R_c^2 + L_d L_q \omega_e^2)^2} \\ C &= \frac{2R_c L_d \Psi_{md} \omega_e^2 (L_q^2 \omega_e^2 + R_c^2)}{(R_c^2 + L_d L_q \omega_e^2)^2} \\ D &= \frac{2R_c^2 L_q \Psi_{md} \omega_e^3 (L_d - L_q)}{(R_c^2 + L_d L_q \omega_e^2)^2} \\ E &= \frac{2R_c^2 L_d L_q \omega_e^3 (L_d - L_q)}{(R_c^2 + L_d L_q \omega_e^2)^2} \\ F &= \frac{R_c \Psi_{md}^2 \omega_e^2 (L_q^2 \omega_e^2 + R_c^2)}{(R_c^2 + L_d L_q \omega_e^2)^2} \end{aligned} \quad (14)$$

If we consider Equation (15) in Equation (14), then Equation (16) is obtained.

$$\begin{aligned} I_d &= I_s \cos \alpha \\ I_q &= I_s \sin \alpha \end{aligned} \quad (15)$$

$$P_{loss, PMSM} = AI_s^2 \cos^2 \alpha + BI_s^2 \sin^2 \alpha + CI_s \cos \alpha + DI_s \sin \alpha + EI_s^2 \sin \alpha \cos \alpha + F \quad (16)$$

The PMSM losses are minimized by Equation (17), yielding Equation (18).

$$\frac{dP_{loss, PMSM}}{d\alpha} = 0 \quad (17)$$

$$\begin{aligned} -2AI_s^2 \sin \alpha \cos \alpha + 2BI_s^2 \sin \alpha \cos \alpha - CI_s \sin \alpha + \\ + DI_s \cos \alpha + EI_s^2 \cos^2 \alpha - EI_s^2 \sin^2 \alpha = 0 \\ -2AI_d I_q + 2BI_d I_q - CI_q + DI_d + EI_d^2 - EI_q^2 = 0 \end{aligned} \quad (18)$$

By rearranging Equation (18) we obtain Equation (19) and consequently Equation (20) which provides the necessary current I_d for every corresponding combination of I_q and ω_e .

$$0 = EI_d^2 + (D + 2I_q(B - A))I_d - (EI_q^2 + CI_q) \quad (19)$$

$$I_{d1,2} = \frac{-D + 2I_q(A - B)}{2E} \pm \frac{\sqrt{(D + 2I_q(B - A))^2 + 4E(EI_q^2 + CI_q)}}{2E} \quad (20)$$

Figure 5 presents the obtained MTPA characteristic by Equation (8), and the obtained ME characteristics by Equation (20) at different values of rotor speed and different values of the iron core resistance R_c . Although, this may not be evident from Figure 5 and similarly to the MTPA characteristics, the ME characteristics are nonlinear. It is however evident from Figure 5 that the iron core resistance R_c plays a crucial role in shaping the ME characteristic. Unfortunately, in practice its value changes depending on operating conditions and it cannot be determined directly or to be given in form of a function.

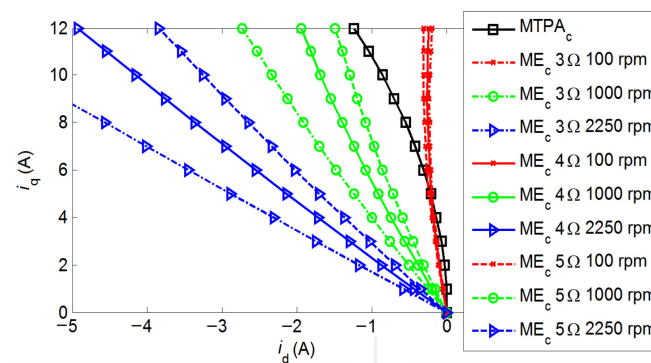


Figure 5. Calculated MTPA and ME characteristics at different rotor speeds and different constant values of the iron core resistance R_c .

Therefore, the authors have turned to an implicit but general approach for determination of the ME characteristic based on experiments, which is described hereinafter. The determined ME characteristics are then used to improve the efficiency of the PMSM drive in sensorless control as well as for the control realization with position sensor. The approach proposed here is novel, and can easily be adopted by control designers when of-the-shelf (or unknown) PMSMs are employed—contrarily to methods based, e.g., on finite element analyses which depend on detailed information about the employed geometry and materials in the PMSM.

3.3. Experimental Determination of ME Characteristics

The ME characteristics derived theoretically in the previous subsections are based on the steady-state PMSM model with constant parameters. With the aim to improve the PMSM drive efficiency and to evaluate the previously presented results, the characteristics were determined also by measurements performed on the PMSM drive, schematically shown in Figure 6. The presented approach includes all effects that are also present during real drive operation in the ME characteristics, these being effects of magnetic nonlinearities, saturation, cross-coupling, end-winding leakage, permanent magnets and slotting, converter nonlinearities and dead times in transistor switching. The PMSM was torque controlled and fed by the inverter. This means that during all tests the d- and q-axis currents were close-loop controlled, following their references set to different constant values. The vector control of PMSM was realized on the control system dSPACE PPC 1103. The rotor speed was closed-loop controlled by an active load IM. The input and output power of the inverter and PMSM, and their efficiencies, were measured by the power analyzers NORMA I (Norma D5255M) and NORMA II (Norma D6100), as shown Figure 6. The equal equipment was used throughout all successive tests, thus enabling a direct and comprehensive comparison of the PMSM drive efficiency operating in closed-loop control with or without the position sensor.

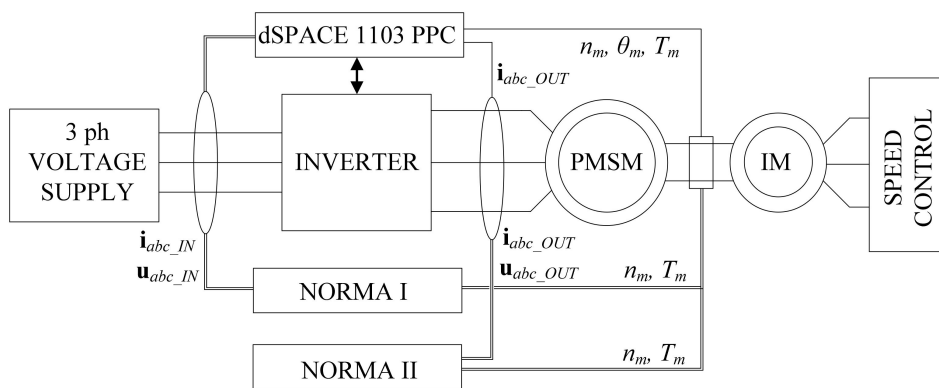


Figure 6. Experimental set-up—schematic presentation.

The ME characteristics were determined by changing the length and angle of the stator current vector at different values of the rotor speed. In individual steady-states, based on the measurements of voltages, currents, powers, torque and speed, the efficiencies are determined. A three-dimensional matrix of measurement results was generated, which includes length and angle of the stator current vector as well as the rotation speed. The experimentally obtained drive efficiency curves at 2250 rpm in dependence of the length and angle of the stator current vector are shown in Figure 7. The ME characteristic at 2250 rpm was then determined by connecting the points of maximum efficiencies of respective efficiency curves (black line). The determined ME characteristics at different rotor speeds are then shown in Figure 8, where they are presented in dependence of d- and q-axis currents. From Figure 8 it is evident that if we want to control the drive with maximum efficiency, the d-axis current component has to be increased by increase of the rotor speed, which is also known as flux-weakening. Unfortunately, due to hardware limitations, only currents of up to 6 A could be achieved during the experiments.

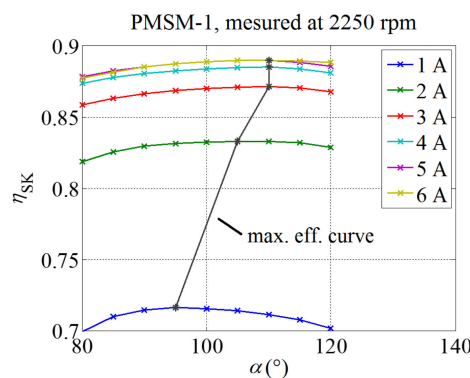


Figure 7. ME characteristic at 2250 rpm in dependence of the length and angle of the stator current vector.

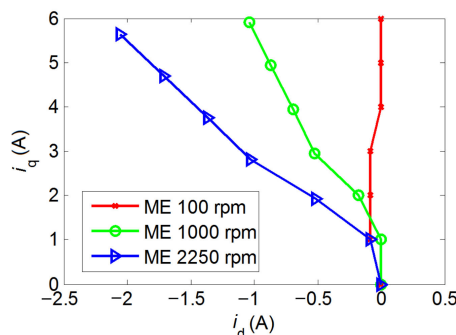


Figure 8. Experimentally determined ME characteristics.

4. Results and Discussion

This section shows how the employment of the previously experimentally determined ME characteristics influences the efficiency of the discussed speed closed-loop controlled PMSM drive, when it is used to generate the d- and q-axis current references. The rotor position and speed required for the control realization are obtained in two different ways: firstly, by using sensors and secondly, by the sensorless control. In the last case, the measured PMSM currents and DC-bus voltage are used together with the PMSM dynamic model to calculate the rotor position and speed. The active flux based sensorless control method is applied. The active flux Ψ_{AF} is defined as a hypothetical flux, which multiplied by the instantaneous q-axis current i_q produces the measured instantaneous electro-magnetic torque t_e [32–35]. Consequently, the effects which are neglected in the PMSM model are thus considered by employment of Ψ_{AF} .

$$t_e = p_p |\hat{\Psi}_{AF}| i_q \quad (21)$$

The active flux concept uses the flux linkage vector estimates $\hat{\Psi}_{\alpha\beta u}$ and $\hat{\Psi}_{\alpha\beta i}$ obtained by the voltage (index u) and current models (index i) (Equation (22)), written in the α - β reference frame [32]. The difference between both estimates gives the compensation voltage u_k , which is added in the voltage model to eliminate the DC-offset and other errors in measured stator currents, variation of stator resistance, and integrator drifts in the calculation procedure.

$$\begin{aligned} \hat{\Psi}_{\alpha\beta u} &= \int_0^t (\mathbf{u}_{\alpha\beta}(\tau) - R_s \mathbf{i}_{\alpha\beta}(\tau) + u_k(\tau)) d\tau + \hat{\Psi}_{\alpha\beta u}(0) \\ \hat{\Psi}_{\alpha\beta i} &= \mathbf{L}_{\alpha\beta} \begin{bmatrix} 1 & 0 \\ 0 & 1 \end{bmatrix} \mathbf{i}_{\alpha\beta} + \mathbf{\Psi}_{md} \begin{bmatrix} \cos \theta_e \\ \sin \theta_e \end{bmatrix} \end{aligned} \quad (22)$$

Considering zero initial conditions, the required estimates of the electrical rotor speed $\hat{\omega}_e$ and position $\hat{\theta}_e$ are calculated by the nonlinear PLL-observer (Equation (23)) [31], where ε represents the error signal; k_1 and k_2 represent the observer gains.

$$\begin{aligned} \hat{\omega}_e &= \int_0^t k_1 \varepsilon(\tau) d\tau \\ \hat{\theta}_e &= \int_0^t (\hat{\omega}_e(\tau) + k_2 \varepsilon(\tau)) d\tau \end{aligned} \quad (23)$$

Thus, in the case of sensorless control, the estimates $\hat{\omega}_e$ and $\hat{\theta}_e$ (Equation (23)) are used instead measured speed and position in the control algorithm, enabling closed loop-speed control without mechanical speed sensor.

Figure 9 shows the schematic presentation of the speed closed-loop control realizations with sensors (position and speed) and without them. These control realizations are applied in the experimental set-up, shown in Figure 6, which is used to measure drive efficiencies in cases when $i_{dr} = 0$, MTPA and ME characteristics, respectively. These characteristics (MTPA or ME) are used to determine the d- and q-axis current references i_{dr} and i_{qr} .

Figure 10 shows the measured PMSM drive efficiencies (η_{ALL}) at the rated speed of 2250 rpm and different loads in the case when $i_{dr} = 0$ and in the cases when i_{dr} and i_{qr} are determined with the MTPA and ME characteristics, respectively. The results are given for the control realization with position and speed sensors and for the sensorless control. They are completed by the presentation of differences between different measured efficiency curves.

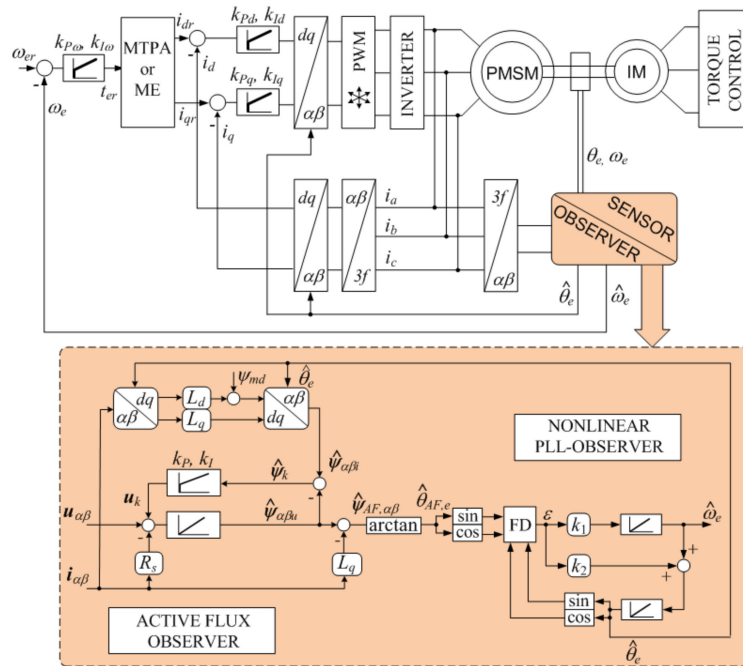


Figure 9. Schematic presentation of the applied speed closed-loop control.

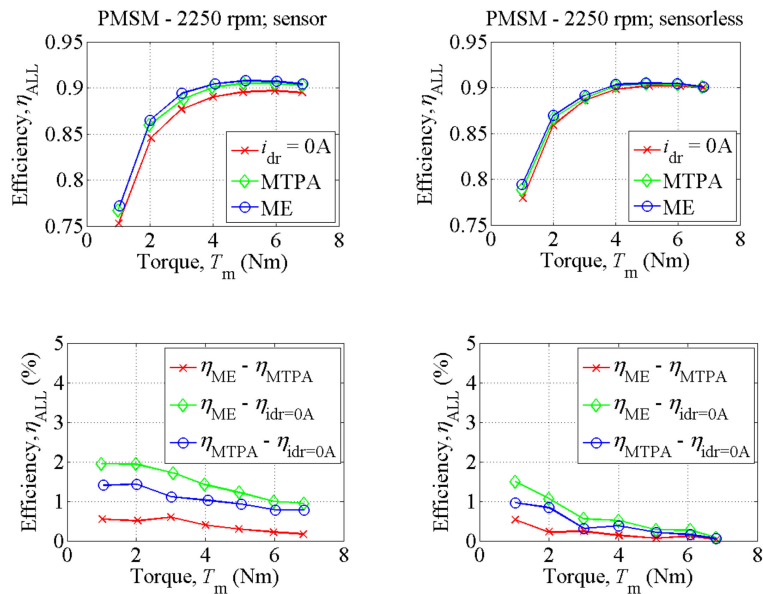


Figure 10. Measured efficiencies of the speed closed-loop controlled PMSM drive and their differences for the control realization with the mechanical sensor and for the sensorless control in the cases when i_{dr} and i_{qr} are determined with MTPA and ME characteristics and in the case when $i_{dr} = 0$.

The presented results clearly show that the lowest efficiencies are achieved when $i_{dr} = 0$. The drive efficiency is improved when the MTPA characteristic is used for the generation of i_{dr} and i_{qr} . When it is replaced with the ME characteristic, the drive efficiency is further improved. Similar findings have been reported in [21,23,28] for an IPMSM drive with position sensor. The efficiency improvements decrease with the increase of the load torque (T_m). This is true for the control realization with the position and speed sensors as well as for the sensorless control realization.

5. Conclusions

This paper presents a way of improving the PMSM drive efficiency, where the more usual $i_{dr} = 0$ and MTPA characteristic for generation of reference current in vector controlled PMSM drives are compared with the proposed ME characteristic. There, both copper and iron core losses of the PMSM are considered. The equations which relate the ME characteristics to the measurable stator currents I_d and I_q which are needed by control designers (instead to the magnetizing currents I_{md} and I_{mq}) are derived, and consequently the equation which provides the optimal current I_d for a given load torque by considering the ME characteristic is obtained for the first time. The problem of adequately determining the iron core resistance parameter value R_c is effectively mitigated by employing experimentally determined ME characteristics on the real PMSM drive system. Differences between the MTPA and ME characteristics are detailed; they are used in speed closed-loop vector control realizations with position and speed sensors and without them. The ME characteristic is implemented in sensorless control for the first time, where a nonlinear PLL observer is applied. Its inputs are calculated by the modified active flux method. The work clearly demonstrates that the use of ME characteristic instead of MTPA characteristic or $i_{dr} = 0$ in the current references generation improves the efficiency of PMSM drive realizations with position and speed sensors and without them—sensorless control.

This particular comparative case study showed that choosing an adequate switching frequency might improve the drive efficiency by 1.5–5.0%. At small load and speed values where the voltage value is small as well, an adequate DC-bus voltage control may improve the drive efficiency up to 30%. Ultimately, this particular PMSM drive efficiency was improved by 0.1–0.5% when the proposed ME was implemented in comparison to the MTPA, and by 1.0–2.0% in comparison to $i_{dr} = 0$, respectively. Therefore, it should be preferred that the PMSM drive control solutions proposed here are implemented in applications where efficiency is crucial. Moreover, the ME implementation can cut down the annual energy consumption of the studied drive by up to approximately 130 kWh, depending on the load and control case presented in Figure 11. This fact certainly cannot be neglected, since its implementation requires merely the modification of a few lines of code in the control realization.

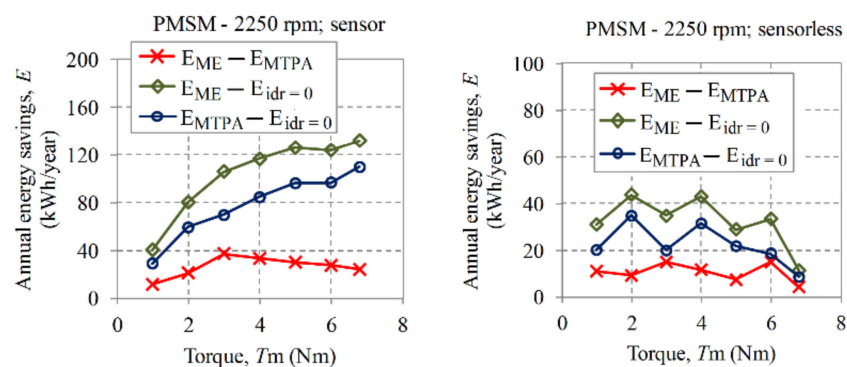


Figure 11. Annual energy savings achieved by different methods of reference current generation in the speed closed-loop controlled PMSM drive for the realization with the mechanical sensor and for the sensorless control.

Author Contributions: Ž.P. performed derivations, experimental work and analyses. T.M. and M.B. prepared the final form of the paper, including editing of the text, equations and figures. G.Š. prepared the experiments and coordinated the research work and paper preparation.

Funding: This work was supported by the Slovenian Research Agency [grant numbers J2-1742, P2-0115].

Conflicts of Interest: The authors declare no conflict of interest.

References

1. Yilmaz, M. Limitations/capabilities of electric machine technologies and modeling approaches for electric motor design and analysis in plug-in electric vehicle applications. *Renew. Sustain. Energy Rev.* **2015**, *52*, 80–99. [[CrossRef](#)]
2. Wang, E.; Guo, D.; Yang, F. System design and energetic characterization of a four-wheel-driven series-parallel hybrid electric powertrain for heavy-duty applications. *Energy Convers. Manag.* **2015**, *106*, 1264–1275. [[CrossRef](#)]
3. Gao, X.Z.; Houn, Z.X.; Guo, Z.; Chen, X.Q. Reviews of methods to extract and store energy for solar-powered aircraft. *Renew. Sustain. Energy Rev.* **2015**, *44*, 96–108.
4. Daili, Y.; Gaubert, J.P.; Rahmani, L. Implementation of a new maximum power point tracking control strategy for small wind energy conversion systems without mechanical sensors. *Energy Convers. Manag.* **2015**, *97*, 298–306. [[CrossRef](#)]
5. Finch, J.W.; Giaouris, D. Controlled AC electrical drives. *IEEE Trans. Ind. Electron.* **2008**, *55*, 481–491. [[CrossRef](#)]
6. Chaoui, H.; Khayamy, M.; Okoye, O. MTPA based operation point speed tracking for PMSM drives without explicit current regulation. *Electr. Power Syst. Res.* **2017**, *151*, 125–135. [[CrossRef](#)]
7. Ancuti, R.; Boldea, I.; Andreescu, G.D. Sensorless V/f control of high-speed surface permanent magnet synchronous motor drives with two novel stabilising loops for fast dynamics and robustness. *IET Electr. Power Appl.* **2010**, *4*, 149–157. [[CrossRef](#)]
8. Krüner, S.; Hackl, C.M. Experimental Identification of the Optimal Current Vectors for a Permanent-Magnet Synchronous Machine in Wave Energy Converters. *Energies* **2019**, *12*, 862. [[CrossRef](#)]
9. Wang, G.; Yang, R.; Xu, D. DSP-based control of sensorless IPMSM drives for wide-speed-range operation. *IEEE Trans. Ind. Electron.* **2013**, *60*, 720–727. [[CrossRef](#)]
10. Chi, W.C.; Cheng, M.Y. Implementation of a sliding-mode-based position sensorless drive for high-speed micro permanent-magnet synchronous motors. *ISA Trans.* **2014**, *53*, 444–453. [[CrossRef](#)]
11. Toman, M.; Dolinar, D.; Štumberger, G. Sensorless control of the permanent magnet synchronous motor. *Electrotech. Rev.* **2004**, *71*, 277–282.
12. Kung, Y.S.; Thanh, N.P.; Wang, M.S. Design and simulation of a sensorless permanent magnet synchronous motor drive with microprocessor-based PI controller and dedicated hardware EKF estimator. *Appl. Math. Model.* **2015**, *39*, 5816–5827. [[CrossRef](#)]
13. Lin, S.; Zhang, W. An adaptive sliding-mode observer with a tangent function-based PLL structure for position sensorless PMSM drives. *Electr. Power Energy Syst.* **2017**, *88*, 63–74. [[CrossRef](#)]
14. Rostami, A.; Asaei, B. A novel method for estimating the initial rotor position of PM motors without the position sensor. *Energy Convers. Manag.* **2009**, *50*, 1879–1883. [[CrossRef](#)]
15. Zhu, Z.Q.; Gong, L.M. Investigation of effectiveness of sensorless operation in carrier-signal-injection-based sensorless-control methods. *IEEE Trans. Ind. Electron.* **2011**, *58*, 3431–3439. [[CrossRef](#)]
16. Wu, X.; Huang, S.; Liu, P.; Wu, T.; He, Y.; Zhang, X.; Chen, K.; Wu, Q. A reliable initial rotor position estimation method for sensorless control of interior permanent magnet synchronous motors. *ISA Trans.* **2019**, in press. [[CrossRef](#)] [[PubMed](#)]
17. Song, Z.; Hou, Z.; Jiang, C.; Wei, X. Sensorless control of surface permanent magnet synchronous motor using a new method. *Energy Convers. Manag.* **2006**, *47*, 2451–2460. [[CrossRef](#)]
18. Omrane, I.; Etien, E.; Dib, W.; Bachelier, O. Modeling and simulation of soft sensor design for real-time speed and position estimation of PMSM. *ISA Trans.* **2015**, *57*, 329–339. [[CrossRef](#)] [[PubMed](#)]
19. Foo, G.; Rahman, M.F. Sensorless sliding-mode MTPA control of an IPM synchronous motor drive using a sliding-mode observer and HF signal injection. *IEEE Trans. Ind. Electron.* **2010**, *57*, 1270–1278. [[CrossRef](#)]
20. Chen, S.Y.; Luo, Y.; Pi, Y.G. PMSM sensorless control with separate control strategies and smooth switch from low speed to high speed. *ISA Trans.* **2015**, *58*, 650–658. [[CrossRef](#)] [[PubMed](#)]
21. Ni, R.; Xu, D.; Wang, G.; Ding, L.; Zhang, G.; Qu, L. Maximum efficiency per ampere control of permanent-magnet synchronous machines. *IEEE Trans. Ind. Electron.* **2015**, *62*, 2135–2143. [[CrossRef](#)]
22. Pan, C.T.; Sue, S.M. A linear maximum torque per ampere control for IPMSM drives over full-speed range. *IEEE Trans. Energy Convers.* **2005**, *20*, 359–366. [[CrossRef](#)]

23. Pohlenz, D.; Böcker, J. Efficiency improvement of an IPMSM using maximum efficiency operating strategy. In Proceedings of the 14th International Power Electronics and Motion Control Conference (EPE/PEMC), Ohrid, Macedonia, 6–8 September 2010; pp. T5-15–T5-19.
24. Hassan, W.; Wang, B. Efficiency optimization of PMSM based drive system. In Proceedings of the 7th International Power Electronics and Motion Control Conference (IPEMC), Harbin, China, 2–5 June 2012; pp. 1027–1033.
25. Wang, M.S.; Hsieh, M.F.; Lin, H.Y. Operational Improvement of Interior Permanent Magnet Synchronous Motor Using Fuzzy Field-Weakening Control. *Electronics* **2018**, *7*, 452. [[CrossRef](#)]
26. Yu, L.; Zhang, Y.; Huang, W. Accurate and Efficient Torque Control of an Interior Permanent Magnet Synchronous Motor in Electric Vehicles Based on Hall-Effect Sensors. *Energies* **2017**, *10*, 410. [[CrossRef](#)]
27. Li, H.; Gao, J.; Huang, S.; Fan, P. A Novel Optimal Current Trajectory Control Strategy of IPMSM Considering the Cross Saturation Effects. *Energies* **2017**, *10*, 1460. [[CrossRef](#)]
28. Cavallaro, C.; Di Tommaso, A.O.; Miceli, R.; Raciti, A.; Galluzzo, G.R.; Trapanese, M. Efficiency enhancement of permanent-magnet synchronous motor drives by online loss minimization approaches. *IEEE Trans. Ind. Electron.* **2005**, *52*, 1153–1160. [[CrossRef](#)]
29. Colby, R.S.; Novotny, D.W. Efficient operation of surface-mounted PM synchronous motors. *IEEE Trans. Ind. Appl.* **1987**, *IA-23*, 1048–1054. [[CrossRef](#)]
30. Morimoto, S.; Tong, Y.; Takeda, Y.; Hirasu, T. Loss minimization control of permanent magnet synchronous motor drives. *IEEE Trans. Ind. Electron.* **1994**, *41*, 511–517. [[CrossRef](#)]
31. Harnefors, L.; Nee, H.P. A general algorithm for speed and position estimation of AC motors. *IEEE Trans. Ind. Electron.* **2000**, *47*, 77–83. [[CrossRef](#)]
32. Boldea, I.; Paicu, M.C.; Andreescu, G.D. Active flux concept for motion-sensorless unified AC drives. *IEEE Trans. Power Electron.* **2008**, *23*, 2612–2618. [[CrossRef](#)]
33. Boldea, I.; Paicu, M.C.; Andreescu, G.D.; Blaabjerg, F. Active flux” orientation vector sensorless control of IPMSM. In Proceedings of the 11th International Conference on Optimization of Electrical and Electronic Equipment (OPTIM), Brasov, Romania, 22–24 May 2008; pp. 161–168.
34. Boldea, I.; Paicu, M.C.; Andreescu, G.D.; Blaabjerg, F. “Active Flux” DTFC-SVM sensorless control of IPMSM. *IEEE Trans. Energy Convers.* **2009**, *24*, 314–322. [[CrossRef](#)]
35. Chen, J.; Chen, S.; Wu, X.; Tan, G.; Hao, J. A Super-Twisting Sliding-Mode Stator Flux Observer for Sensorless Direct Torque and Flux Control of IPMSM. *Energies* **2019**, *12*, 2564. [[CrossRef](#)]
36. Di Piazza, M.C.; Pucci, M. Techniques for efficiency improvement in PWM motor drives. *Electr. Power Syst. Res.* **2016**, *136*, 270–280.
37. Ghaeb, J.A.; Smadi, M.A.; Ababneh, M. Progressive decrement PWM algorithm for minimum mean square error inverter output voltage. *Energy Convers. Manag.* **2011**, *52*, 3309–3318. [[CrossRef](#)]
38. Marčič, T.; Štumberger, G.; Hadžiselimović, M.; Zagradišnik, I. The impact of modulation frequency on losses, current harmonic distortion and motor temperature in an induction motor drive. *Electrotech. Rev.* **2006**, *73*, 125–130.

